Publication P6

Jere Kolehmainen. 2010. Synchronous reluctance motor with form blocked rotor. IEEE Transactions on Energy Conversion, volume 25, number 2, pages 450-456.

Synchronous Reluctance Motor With Form Blocked Rotor

Jere Kolehmainen, *Member, IEEE*

***Abstract*—A novel type of mechanically robust synchronous reluctance rotor structure is proposed for medium speed synchronous reluctance machines. A machine utilizing the construction is built, tested, and compared to another machine with the common synchronous reluctance rotor structure. The machine is also simulated using the finite element method and the results are compared to the tested values. The obtained results demonstrate the feasibility of the construction.**

***Index Terms*—Electromagnetic analysis, synchronous machines, variable-speed drives.**

I. Introduction

INVERTER-DRIVEN synchronous reluctance motors are a good choice for many variable-speed drive systems. Today's variable-speed industrial drives are mostly based on standard two or four-pole induction motors. These applications are also suitable for synchronous reluctance motors. The first rotating-magnetic-field synchronous motor was, however, introduced by Kostko in 1923 [1]. Traditionally, synchronous reluctance motors are used directly online with a rotor cage, because pure synchronous reluctance motors do not have a starting torque characteristic [2], [3]. Nowadays, by using modern inverter technology, suitable field-oriented control and a pulsewidth modulation (PWM) technique, the machine without the rotor cage can still be started.

The advantages of the synchronous reluctance motors with variable-speed drive are mentioned in [4]. They are of simple rotor construction with no vital need for the rotor cage in speed-controlled drives, have no rotor resistive losses, with low-inertia, synchronous running and easy speed control without encoders. They also have easy field weakening compared to synchronous permanent-magnet motors. Although, synchronous permanent-magnet motors are also a good choice for many variable-speed drive applications, the advantages of using synchronous reluctance motors, as opposed to permanent-magnet motors, is that expensive magnets are not needed. However, it is also introduced permanent magnets-assisted synchronous reluctance machines where properties of synchronous reluctance and permanent magnet machines are combined [5].

An additional benefit of synchronous reluctance motors is material saving. They could be produced with similar kinds of methods as synchronous permanent-magnet motors and induction motors. However, there are many difficulties in producing them, such as complex structures and costly machining.

Manuscript received November 28, 2007; revised February 17, 2009; accepted December 1, 2009. Date of publication February 2, 2010; date of current version May 21, 2010. This work was supported in part by the ABB Oy, Motors, Finland. Paper no. TEC-00475-2007.

The author is with the ABB Oy, Motors, Vaasa FIN-65101, Finland (e-mail: jere.kolehmainen@fi.abb.com).

Digital Object Identifier 10.1109/TEC.2009.2038579

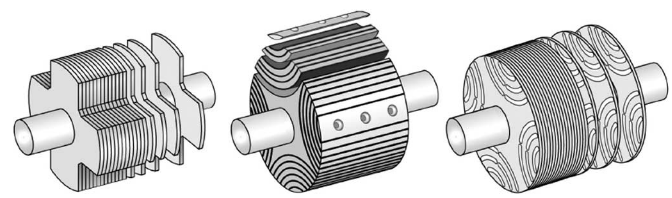

(a) (b) (c)

Fig. 1. Schematics of (a) simple salient pole, (b) axially laminated, and (c) transversally laminated rotors.

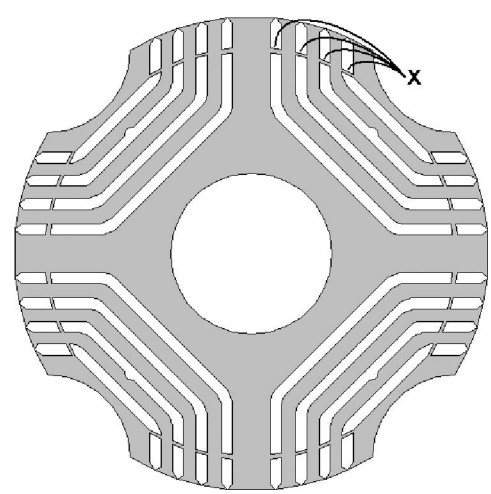

Fig. 2. Rotor design with bridge-fixed poles. Four of the supporting bridges are marked with "x."

The major types of synchronous reluctance rotors (see Fig. 1) are the simple salient pole rotor [6], the transverse laminated rotor [1], [7] and the axially laminated rotor [8], [9]. The salient pole rotor design has a simple and rigid structure but a low saliency ratio and consequently poor performance. However, the rigid structure gives a possibility to use the salient pole rotor design in high-speed machines [6]. The axially laminated rotor design has a good saliency ratio and performance, but eddy current losses due to the axial lamination are larger. However, the mechanical design is extremely complex for industrial manufacturing. Axially laminated structures of the two-pole rotor can also be produced by explosive bonding [10]. In practice, the transversally laminated rotor design is the best choice for industrial manufacturing, for example, for frame size 280 mm as will be explained.

The typical way of manufacturing a transverse laminated rotor is to assemble a stack of punched or laser-cut rotor disks with flux paths. The flux paths are fixed to the rest of the rotor structure with thin iron bridges (for example, see detail "x" in Fig. 2). The disadvantage of the supporting bridges is the flux

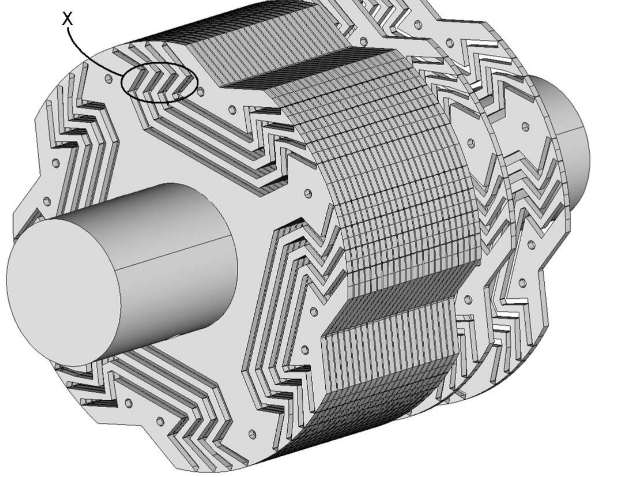

Fig. 3. Schematic of the new design with dovetail shaped poles without supporting bridges. One of eight supporting filler areas is marked with “x.”

leakage, the magnitude of which depends on the thickness of the bridges. In low-speed applications, this is not a problem since the centrifugal forces acting on the poles are relatively small and the bridges can be kept thin. However, as the tangential speed of the rotor surface in higher speed applications (3000–8000 r/min) exceeds 50 m/s (which corresponds to 3200 r/min in motor size IEC280) the stresses in the bridges will exceed the yield strength of the electrical steel (which is typically 305 MPa for grade M400-50 A). This problem can be countered by increasing the thickness of the bridges, however, this increases the flux leakage, which in turn increases the magnetization current needed to get the required torque.

In this paper, we study a solution on how to get mechanically more robust transverse laminated rotor structures without using supporting iron bridges. In the solution, the tensile stress is geometrically converted into a compressive one, and also the extra filling material is used to support the pole structure. Thus, the form of the structure supports the rotor against centrifugal forces. Furthermore, a new structure of transverse laminated rotor is presented [11]. In the structure, the outer parts of the rotor are supported by the inner parts using epoxy adhesive between the parts. An example of a new dovetail design is shown in Fig. 3. Previously, some dovetail-type supporting rotor solutions were considered for permanent-magnet synchronous motors [12]–[14].

The new dovetail solution is compared to a traditionally used solution with supporting bridges (see Fig. 2). The electrical comparison is done using time-stepping calculations with the finite element method (FEM) [15]. The mechanical comparison is done using strength calculations with FEM [16]. Motors with both rotor designs are built and tested. The motor with the dovetail design is analyzed further and results are compared to simulations.

II. Motor Designs

A four-pole motor with bridge-fixed rotor design is used as an example for comparison with a motor with the new dovetail design. The only difference between the two motors is in their rotor structure. The rotor geometries can be seen in Figs. 2 and 3, respectively. In the both designs, the pole consists of four flux barriers. Flux barriers are long white areas in Fig. 2 and long holes in Fig. 3. In addition, the bridge-fixed design has two supporting bridges in every flux barrier while no supporting bridges are needed in the dovetail design. As the centrifugal force pushes the flux paths outward, the inner flux paths and the epoxy between the paths lock the pole firmly in place and prevent it from moving. One of eight essential areas for supporting the flux paths against centrifugal force is marked with “x” in Fig. 3. In those areas, holes are filled with the filler material and compressive force is the dominant force in the filler material. Therefore, the form of the structure locks the pole firmly in place. Also antiadhesive filler materials can be used.

Although, epoxy materials are rather soft compared to electrical sheets, the epoxy layers tolerate compressive stress well (up to 15–21 MPa). At the same time, the large contact area between the pole wedge and the epoxy renders the compressive stress to an acceptable level.

The motors under study are designed to work at a speed of 1500 r/min with a torque of 573 N·m. However, the motor with the dovetail rotor design sustains with higher speeds. The common machine data is shown in Table I.

TABLE I
Nominal Values and Main Dimensions of Studied Machines

Quantity	Value
Shaft height (mm)	280
Power (kW)	90
Torque (Nm)	573
Voltage (V)	440
Current (A)	160
Speed (1/min)	1500
Stator outer radius (mm)	460
Stator inner radius (mm)	295
Stack length (mm)	250
Air gap (mm)	1.2
Number of poles	4
Number of slots per pole per phase	6
Connection	Delta
Number of effective conductors in slot	5
Number of parallel branches	2

III. Rotor Manufacturing

One machine with each rotor type is manufactured. The normal method to manufacture the rotor (which is to assemble a stack of disks, compress it using bolts and nonmagnetic end plates and shrink fit the stack onto the shaft), is used for manufacturing the rotor with bridge-fixed design.

In the dovetail design without any supporting bridges, the disks are first cut with iron bridges in the air gap. Then, as with bridge-fixed design, a stack of discs is assembled, compressed using bolts and nonmagnetic end plates, and shrink-fitted onto the shaft. After that, the flux barriers are filled with epoxy adhesive. Finally, all supporting iron bridges in the air gap are machined away. The manufactured rotor with the dovetail design can be seen in Fig. 4.

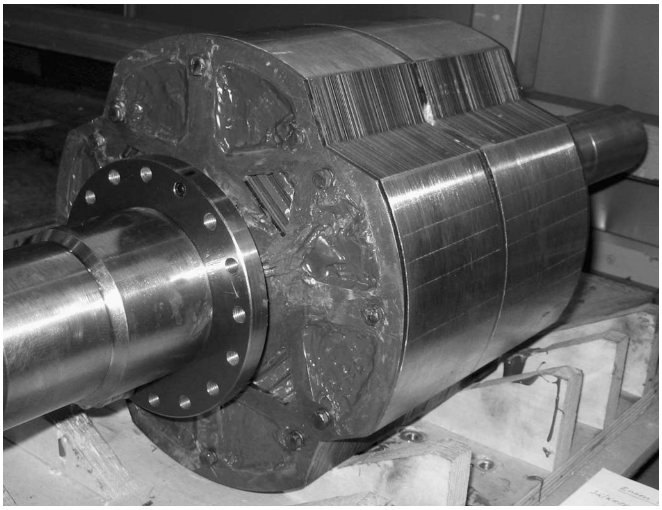

Fig. 4. Dovetail rotor after epoxy adhesive filling and machining.

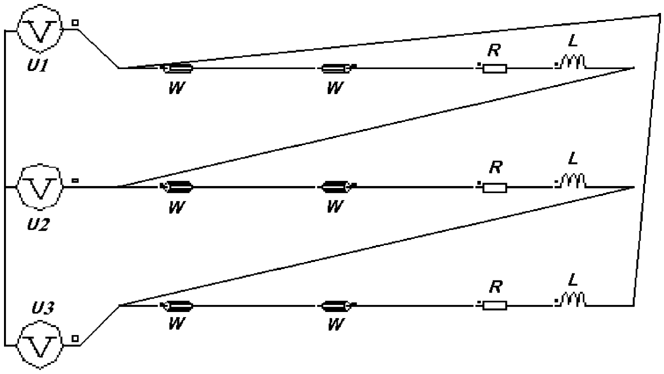

Fig. 5. Flux2D circuit used in the calculations.

IV. Electric Simulation Results

The electrical properties of the motors with the bridge-fixed design in Fig. 2 and the dovetail design in Fig. 3 are studied with FEM. The simulations are done in voltage source operation mode using Flux2D software by Cedrat Research [15]. A delta connection is used. The circuit diagram of voltage source calculations is shown in Fig. 5. In the circuit, there are three voltage sources $U1$, $U2$, and $U3$, six windings W and three end-winding resistances R and three end-winding inductances L. In all time stepping calculations with voltage source, the form of the voltage form is sinusoidal. Simulations are started with various rotor angles and stopped after 40 electrical periods when transient oscillations have totally died away. Constant rotor speed is used.

In efficiency calculations, electromagnetic and friction losses are taken into account. Iron losses are calculated with the following:

$$P_{\mathrm{TOT}} = k_h B_m^2 f + \frac{1}{T}\int_0^T \left[\sigma \frac{d^2}{12}\left(\frac{dB}{dt}(t)\right)^2 + k_e \left(\frac{dB}{dt}(t)\right)^{3/2}\right] k_f \, dt \qquad (1)$$

TABLE II
Comparison of Measured and Calculated Parameters for the Dovetail and Bridge Fixed Design

Quantity	Dovetail, Evaluated	Dovetail, Measured	Bridge fixed, Evaluated	Bridge fixed, Measured
Shaft Power (kW)	90	90	90	90
Torque (Nm)	573.0	573.1	573	572.6
Voltage (V)	440.0	440.1	440.0	440.1
Current (A)	173.4	186.6	159.6	175.7
Efficiency (%)	95.6	93.3	95.9	95.1
Power factor	0.743	0.678	0.797	0.706
Total Losses (W)	4183	6470	3810	4680
Copper losses (W)	2141	2241	1817	1987
Iron losses (W)	1442	3629	1393	2093
Friction losses (W)	600	600	600	600
No load current (A)	71.2		53.0	
Max torque (Nm)	905.8		1110.7	

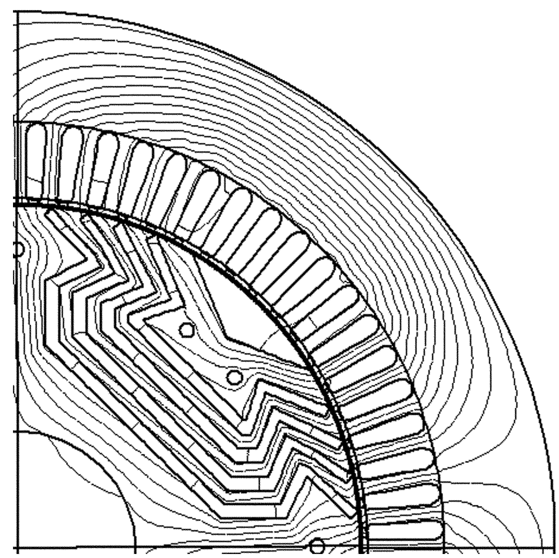

Fig. 6. Concentration of flux in the dovetail design at nominal operating point.

where B_m, f, σ, d, k_h, and k_e are the maximum flux density at the node concerned, the frequency, the conductivity, the lamination thickness, the coefficient of hysteresis loss, and the coefficient of excess loss, respectively.

First, the nominal load states of the designs are defined with time stepping simulations and different load angles. Evaluated nominal load values are shown in Table II. With the dovetail design, nominal current is 8.6% greater and load angle is 5.3° (= 38.7° – 33.4°) greater, consequently copper losses are larger and the power factor is smaller than with the bridge-fixed design.

As the rotor structures have different flux routes, flux distributions differ inside the rotors and this has an effect also on the flux distributions of the whole motors. For studying this difference, flux lines at nominal load are shown in Figs. 6 and 7. The flux concentrates on one side of the pole and the difference in leakage fluxes in the rotors can be seen. With the bridge-fixed design, part of the flux leaks through the bridges and the dovetail rotor has larger leakage flux through flux barriers.

Furthermore, flux densities in a single stator tooth, at nominal load of both the dovetail and the bridge-fixed designs are shown

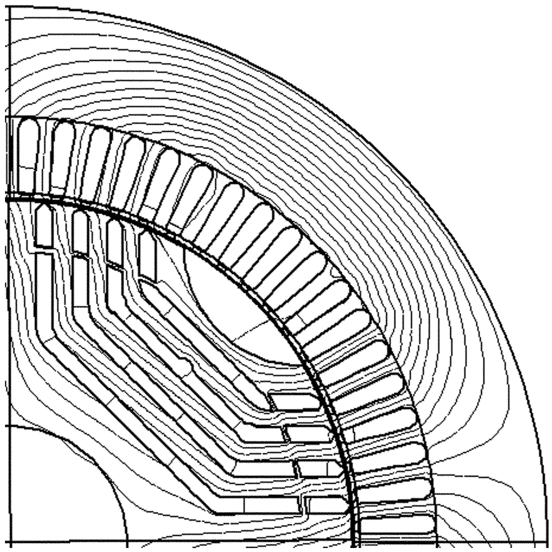

Fig. 7. Concentration of flux in the bridge-fixed design at nominal operating point.

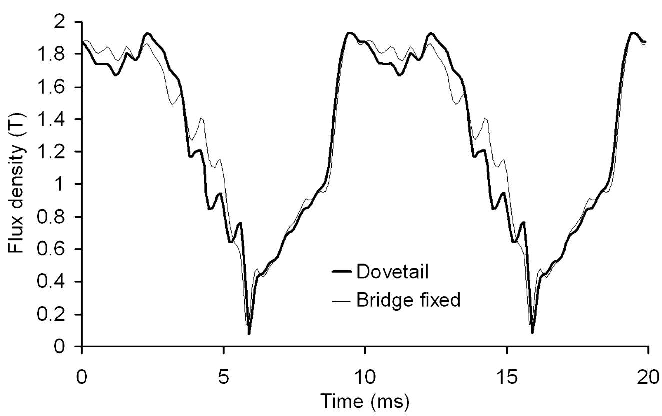

Fig. 8. Absolute flux densities in the stator teeth of the dovetail and the bridge-fixed designs at the same load angle near nominal load and speed 1500 r/min as a function of time.

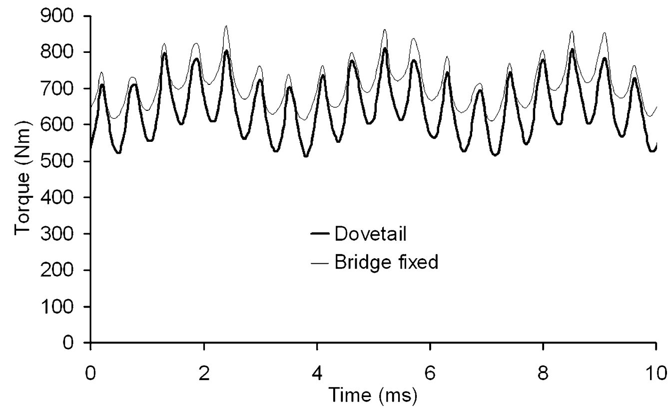

Fig. 9. Torque oscillations in the bridge fixed and the dovetail designs at same load angle near nominal load and speed 1500 r/min as a function of time.

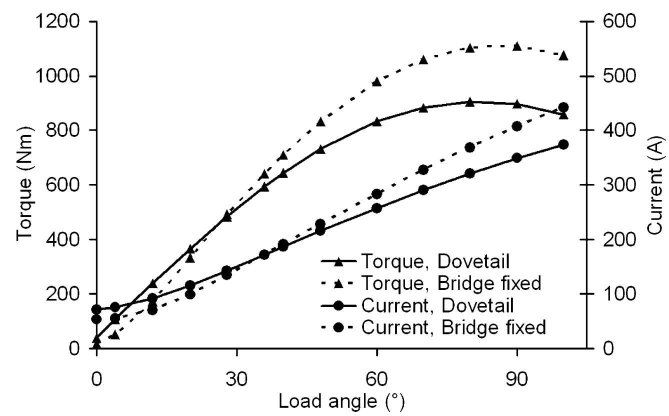

Fig. 10. Calculated torque and current of the dovetail and the bridge-fixed design as a function of load angle.

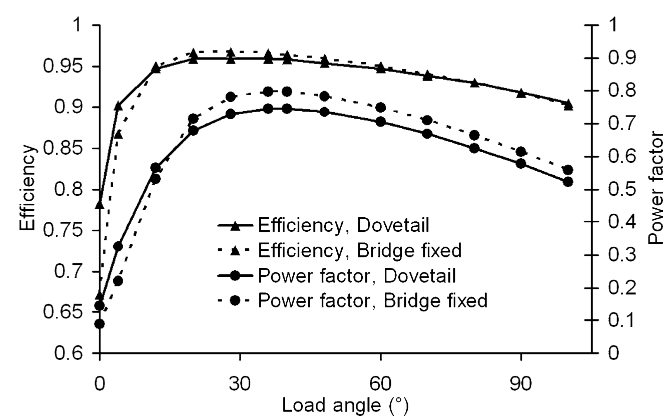

Fig. 11. Calculated efficiency and power factor of the dovetail and the bridge-fixed design as a function of load angle.

in Fig. 8 as a function of time. Average flux in a stator tooth is 1.3% larger with the bridge-fixed design. The effect on the flux density distribution, caused by the larger reluctance of flux paths between flux barriers and the smaller reluctance of the skeleton area, can be seen as two clear maximums in one period. This affects also the torque oscillation as can be seen in Fig. 9. Thus, at nominal load, a different flux concentration in the dovetail design results in a larger torque oscillation. In the bridge-fixed design, there is a 7.0% torque oscillation coming from the stator slots. The dovetail design increases this oscillation to 10.1%, although this oscillation can be reduced also with skewing [17]. However, our designs are not skewed. In the bridge-fixed design, the average torque oscillation over one slot, which roughly approximates the effect of skewing, is slightly larger than in the dovetail design, (6.0% and 4.6%, correspondingly).

The calculated electrical properties as a function of electric load angle are compared in Figs. 10 and 11. With the dovetail design, torque is higher with small load angles because of smaller flux leakage and smaller with large load angles because of larger reluctance on direct axis. Consequently, with the dovetail design, the maximum torque of 906 N·m at load angle 82.1° is smaller than the maximum torque of 1111 N·m at load angle 86.3° with the bridge-fixed design.

However, current differences behave contrary to torque differences in the designs. Furthermore, the current is smaller with small and larger with large load angles with the dovetail design. Consequently, with the dovetail design, power factor and

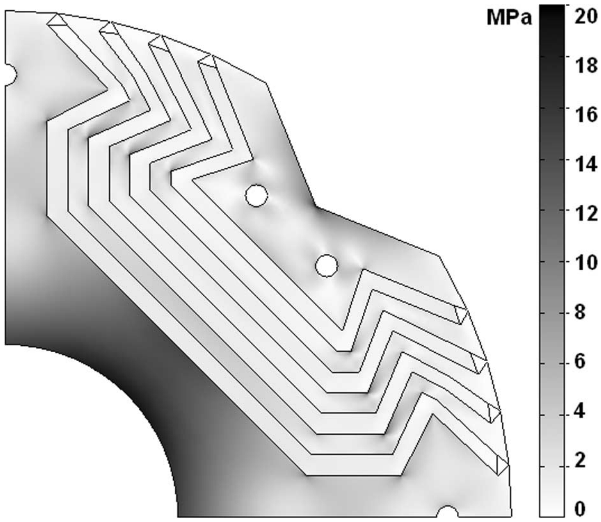

Fig. 12. Von Mises stress in the rotor with dovetail design, at speed 3000 r/min.

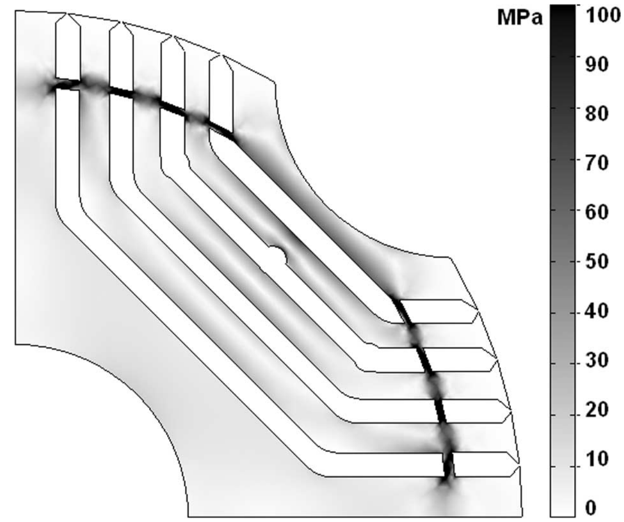

Fig. 13. Von Mises stress in the rotor with bridge-fixed design, at speed 3000 r/min.

efficiency are larger with electric load angles under 16° and 12° and smaller with higher load angles. However, both power factor and efficiency are better in the whole power range with the bridge-fixed design, because lower load angles are needed. Although the modeled electrical properties are worse with the dovetail design, they are sufficient for the intended use. In conclusion, mechanical strength is increased at the cost of electrical properties.

V. Force Computation

The dovetail rotor has a totally different stress distribution compared to the bridge-fixed rotor. In the bridge-fixed rotor, most of the shear and tension stresses are in the iron bridges, whereas in the dovetail design, most of stresses are compression stresses in the epoxy adhesive layers between flux paths and shear stresses near the corners of flux barriers.

Von Mises stresses in the dovetail and bridge-fixed designs are modeled with FEM [16]. Computations are done using the centrifugal force associated with a speed of 3000 r/min. Stress distributions are shown in Figs. 12 and 13, respectively. In the figures, stresses are greatest in dark gray areas. Note different scales between figures.

With bridge-fixed design, the largest stress 288 MPa is in the bridges of electrical steel sheet. This value is near the yield strength (305 MPa) of the steel. The maximum speed of rotors designs can be approximated with the following:

$$n_{\max} = n_{\mathrm{calc}} \sqrt{\frac{\sigma_{\mathrm{yield}}}{R_{\mathrm{calc}} \eta}} \tag{2}$$

where $n_{\max}, n_{\mathrm{calc}}, \eta, \sigma_{\mathrm{yield}}$ and R_{calc} are maximum speed, calculation speed, factor of safety, yield strength, and calculated critical stress.

Using safety factor of 1.5, the maximum speed of the bridge-fixed design is 2521 r/min. With the dovetail design, the largest stress, 78 MPa, is localized in the corners of the sheets. These values are below the yield strength (305 MPa) of the steel. The largest stress on the supporting epoxy adhesive layer, 6 MPa, is localized in the corners of the supporting area. It is also well below the lap shear strength of the epoxy adhesive (Araldite 2104) as 15–21 MPa with temperature area – 40 to 100 °C. (The lap shear strength of Araldite 2014 is under 6 MPa with temperatures over 140 °C). Therefore, the strength of the epoxy adhesive defines the maximum speed of the dovetail rotor as 3873 r/min with a safety factor of 1.5. In conclusion, using the dovetail design to stabilize the structure, it becomes robust enough for the speed of 3800 r/min with epoxy adhesive temperature under 100 °C, while it was 2500 r/min with the bridge-fixed design.

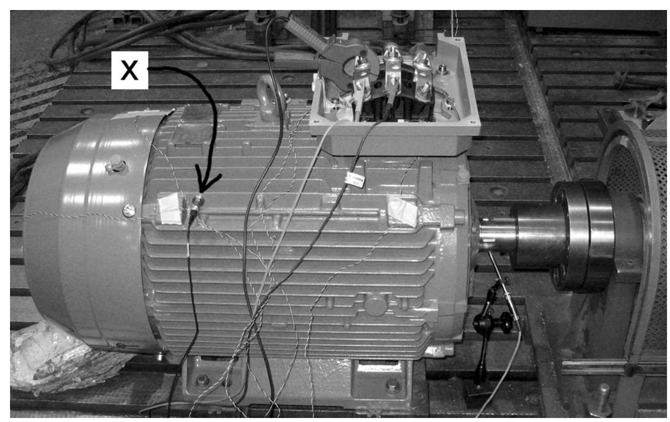

Fig. 14. Test arrangement. Vibration sensor is marked with "x."

VI. Test Results

One motor with each rotor type is tested. For all tests with different loads, sinusoidal supply voltage is used. In practice, for industrial utilization, the control strategy with software for synchronous reluctance ac machines with frequency converters should be used. The load tests are done with a load machine. Motors with both designs are tested with different loads at a speed of 1500 r/min. The test arrangement can be seen in Fig. 14. In addition, for the motor with the dovetail design, no-load tests

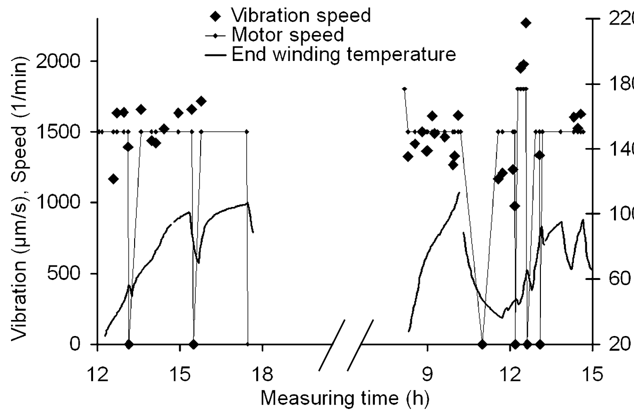

Fig. 15. Relative vibration level during load tests of the motor with the dovetail rotor as a function of measuring time. Also rotor speed, output power, and stator end winding temperature rise are shown.

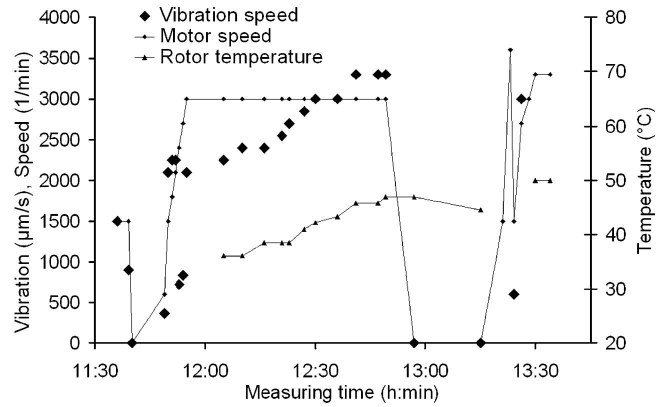

Fig. 16. Relative vibration level during no load tests of the motor with the dovetail rotor as a function of measuring time. Also rotor speed and approximated rotor temperature are shown.

were performed up to 3600 r/min, without the load machine, but with frequency converter and frequency control.

The mechanical durability test of the motor with the dovetail rotor contains four parts. The first three parts are performed with a load machine and different loads. The test history of the first parts with motor speed, power and relative vibration level is shown in Fig. 15. A measurement point of the vibration level is on “top corner” of the frame and the measurement angle is 45° from tangential direction of the frame. The point is marked with “x” in Fig. 14. First, the motor is tested at different loads running at 1500 r/min. After this, the load is set to the nominal level and the motors are run for four hours. Then the motor is cooled down for 14 h. Next, load tests are done by running the motors at 1800 r/min for 3 min. The, relative vibration level remains the same over all measurements at the same speed. This indicates that the dovetail rotor maintains its balance. Also subsequential measurements give evidence that, as the vibration level was stationary; there is no plastic deformation in the rotor sheets and epoxy layers.

In the last over-speed test without the load machine, the motor was run at 3000 r/min. The vibration stayed at the same level as in the 1500 r/min test. Hence, the dovetail rotor maintains its shape with at 3000 r/min. Also, rotation speeds of 3300 and 3600 r/min are tested. Vibration history is shown in Fig. 16. Although vibration level remained small, during the test, at 3600 r/min the motor finally broke down. Subsequential measurements showed two local small plastic deformations in the rotor. In these deformation spots, small amounts of epoxy adhesive had melted and were thrown out into the air gap.

In conclusion, the tested rotor sustained speeds up to 3000 r/min. With some other type of adhesive materials, higher speeds could be reached.

For choosing the best supply voltage with nominal power and speed, the electrical properties of the machine with the dovetail design are measured with different supply voltages. Power factor, efficiency, and power/current ratio are shown as a function of supply voltage in Fig. 17. Measured maximum of power factor, efficiency, and torque/current ratio are with

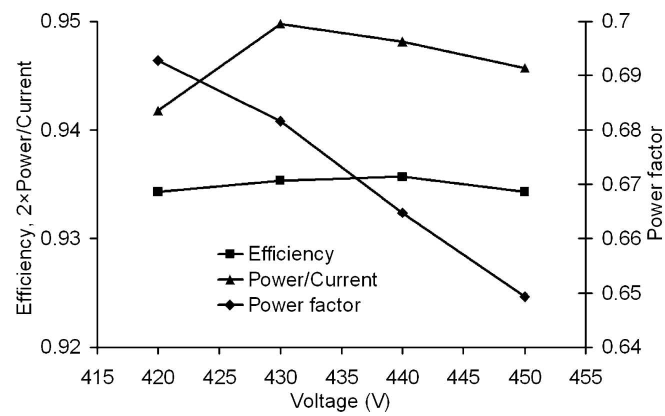

Fig. 17. Measured power factor, efficiency and power current ratio as a function of terminal voltage.

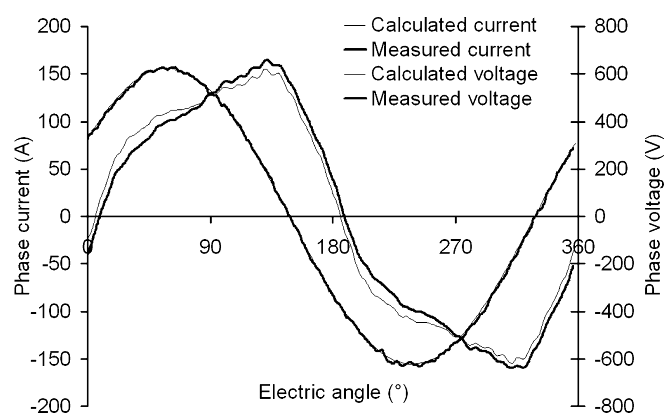

Fig. 18. Calculated and measured voltage and current of the dovetail design as a function of load angle.

voltages 440, 430, and 420 V, respectively. Therefore, voltage 440 V is chosen for the following studies.

For validating the calculation model, the measured phase current as a function of electric angle is compared with modeled one with the load angle 40°, which gives load near nominal. In the comparison shown in Fig. 18, the electric angles are shifted axially so that voltages overlap each other. Similar behavior of

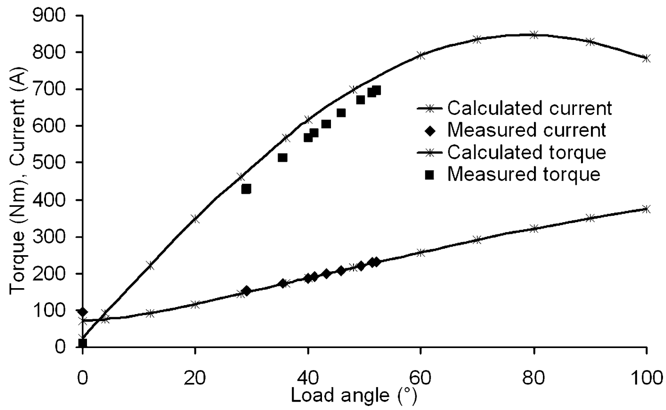

Fig. 19. Calculated and measured torque of the dovetail design as a function of load angle.

measured and calculated currents can be seen. Electric angles of small current ripple due to slot harmonics are the same as they should be. This also ensures that load angles between the measurement and the calculation are the same. Modeled current curve distortion is slightly smaller, because of the limitations of the 2-D FEM [15], which does not take into account 3-D effects and proper effects of iron losses. Also, electric angles of phase current differs 3.5° (= measured 38.1° – calculated 34.6°).

The measured torque and line current as a function of load angle is compared with the calculated results in Fig. 19. With the same load angles, the actual motor has almost the same measured currents and slightly lower measured torques than in the calculations.

Finally, measured nominal values of both machines with dovetail and bridge-fixed design are compared to evaluated values in Table II. Both calculated line currents are 7.1% (dovetail) and 9.2% (bridge-fixed) smaller than measured. Similarly, calculated power factors are smaller. The most remarkable difference is 55% larger measured losses with the dovetail design (while they are 23% larger with the bridge-fixed design). This indicates that whether real iron losses or friction losses are larger, all friction losses are approximated with the same value in the Table II.

Despite differences between measurements and calculations shown in Figs. 18 and 19 and in Table II, the accuracy of the simulations is sufficient for the comparison of different rotor structures.

VII. Conclusion

The prototype motor with dovetail-shaped flux barriers in the poles exhibits a significant increase in mechanical stability over the conventional bridge-fixed pole design. By converting the tensile and shear stresses in the iron bridges into a compressive stress to the epoxy filler in flux barriers and iron in flux paths by redesigning the pole geometry, a very robust construction can be achieved. The electrical properties can be kept almost at the same level as in the bridge-fixed design. In practice, this dovetail rotor design gives a viable solution to increase the speed range of synchronous reluctance machines with a transversally laminated rotor structure. Our design requires no extra supporting structures to counter the centrifugal forces and is consequently more straightforward to manufacture.

In conclusion, the dovetail design gives an opportunity to increase speed and power range of the transverse laminated rotor solution with the manufacturing method well suitable for industrial production.

Acknowledgment

The author would like to thank J. Ikäheimo, ABB Oy, Motors, for his support and collaboration, and M. Pemberton, ACC Global, for his help in revising the English language of this paper.

References

[1] J. K. Kostko, "Polyphase reaction synchronous motors," *J. Amer. Inst. Elec. Ing.*, vol. 42, pp. 1162–1168, Nov. 1923.

[2] T. A. Lipo and P. C. Krause, "Stability analysis of a reluctance synchronous machine," *IEEE Trans. Power Appl. Syst.*, vol. PAS-86, no. 7, pp. 825–834, Jul. 1967.

[3] T. A. Lipo, "Synchronous reluctance machine, a viable alternative for AC drives," *Elect. Mach. Power Syst.*, vol. 19, pp. 659–671, 1991.

[4] T. J. E. Miller, A. Hutton, C. Cossar, and D. A. Staton, "Design of a synchronous reluctance motor drive," *IEEE Trans. Ind. Appl.*, vol. 27, no. 4, pp. 741–749, Jul. 1991.

[5] I. Boldea, L. Tutelea, and C. I. Pitic, "PM-assisted reluctance synchronous motor/generator (PM-RSM) for mild hybrid vehicles: Electromagnetic design," *IEEE Trans. Ind. Appl.*, vol. 40, no. 2, pp. 492–498, Mar./Apr. 2004.

[6] M.-I. Lamghari-Jamal, J. Fouladgar, E.-H. Zaim, and D. Trichet, "A magneto-thermal study of a high speed synchronous reluctance machine," *IEEE Trans. Magn.*, vol. 42, no. 4, pp. 1271–1274, Apr. 2006.

[7] A. Vagati, "Synchronous reluctance electrical motor having a low torque ripple design," U.S. Patent No. 5818140, Oct. 6, 1998.

[8] A. J. O. Cruickshank, R. W. Menzies, and A. F. Anderson, "Axially laminated anisotropic rotors for reluctance motors," *IEE Proc.*, vol. 113, no. 12, pp. 2058–2060, 1966.

[9] D. Platt, "Reluctance motor with strong rotor anisotropy," *IEEE Trans. Ind. Appl.*, vol. 28, no. 3, pp. 652–658, May 1992.

[10] H. Hofmann and S. R. Sanders, "High-speed synchronous reluctance machine with minimized rotor losses," *IEEE Trans. Ind. Appl.*, vol. 36, no. 2, pp. 531–539, May 1992.

[11] J. Kolehmainen, "Rotor for electric machine," Patent FI 118 940 (B1), May 15, 2008.

[12] J. Kolehmainen and J. Ikäheimo, "Motors with buried magnets for medium speed applications," *IEEE Trans. Energy Convers.*, vol. 23, no. 1, pp. 86–91, Mar. 2008.

[13] J. Kolehmainen, "Machine with a rotor structure supported only by buried magnets," presented at the Int. Symp. Electromag. Fields Elect. Eng. (ISEF), Prague, Czech Republic, Sep. 2007.

[14] S. Wiak, A. Krawczyk, and I. Dolezel, Eds., "Advanced computer techniques in applied electromagnetics," vol. 30, in *Studies in Applied Electromagnetics and Mechanics*. Amsterdam, The Netherlands: IOS Press, 2008, pp. 240–246.

[15] Flux2D^{TM} software. (2007). [Online]. Available: http://www.cedrat.com

[16] FEMLAB^{TM} 3.0 software. (2007). [Online]. Available: http://www.comsol.com

[17] X. B. Bomela and M. J. Kamper, "Effect of stator chording and rotor skewing on average torque and torque ripple of reluctance synchronous machine," in *Proc. IEEE Africon 1999*, vol. 2, pp. 678–690.

Jere Kolehmainen (M'09) received the M.Sc. and Ph.D. degrees in theoretical physics from the University of Jyväskylä, Jyväskylä, Finland in 1996 and 2000, respectively.

He is currently working at ABB Oy, Motors, Vaasa, Finland. His research interests include synchronous and induction ac machines and electromagnetic modeling.